H-H interactions in Nb/W(110) superlattices

Stefan Olsson* and Björgvin Hjörvarsson
Materials Physics, Uppsala University, 751 21 Uppsala, Sweden

Erik B Svedberg
Seagate Technology, 15203 Pittsburgh, Pennsylvania

Kenji Umezawa
Department of Materials Sciences, Osaka Prefecture University, 599-8531 Osaka, Japan
(Received 7 August 2001; revised manuscript received 11 June 2002; published 31 October 2002)

The elastic interaction of hydrogen in Nb/W(110) superlattices and the effect of biaxial compressive strain of the Nb layers on the hydrogen lattice-gas to hydrogen lattice-liquid ($\alpha-\alpha'$) phase boundary are explored. The epitaxial growth of Nb on W introduces biaxial compressive strain in the Nb layers and the degree of compression is governed by the thickness ratio of the constituents. Hydrogen solubility isotherms of four samples of increasing W-layer thickness ($D_W=3-18$ ML) and a constant Nb-layer thickness (12 ML) were measured by combining resistivity measurements and the $^1H(^{15}N,\alpha\gamma)^{12}C$ nuclear reaction. $\Delta\overline{H}_H$ and $\Delta\overline{S}_H$ as functions of the hydrogen concentration and W-layer thickness were deduced. The H-H-interaction was found to depend strongly on the initial strain of the Nb host-lattice. The critical temperature for the α-α' transition was determined to be 287 K for the sample with least compressed Nb layers ($D_W=3$), while no transition of this kind is verified for the other samples.

DOI: 10.1103/PhysRevB.66.155433 PACS number(s): 68.65.Cd, 62.20.Dc, 64.75.+g, 64.70.−p

I. INTRODUCTION

The lattice-gas to lattice-liquid transition of hydrogen (H) in metals, is theoretically treated by Wagner *et al.*[1] The driving force of the transition is of elastic nature and is in principle of infinite range. Hence, size and shape of the absorbing material does effect the modes of the spinodal decomposition, which also has been experimentally verified, e.g. in single crystals of Nb by Zabel and Peisl.[2] H solubility measurements in thin metal films have also been used to address the relation between finite-size effects and elastic boundary conditions.[3,4] The thicknesses of the films were typically in the range: $10-1000$ nm.

Studies of H in multilayers and superlattices with large differences in H-absorption potential of the constituents, is one possible route to determine the H-H-interaction in very thin layers (i.e. typically below 20 atomic monolayers).[5] Nb/W-superlattices are examples of structures of this type, i.e. all absorbed H will be confined in the Nb-layers within a broad temperature range.

Song *et al.*[3] have demonstrated a strong film thickness-dependence of the H-H-interaction in 30-520 nm Nb(110)-films, and predicted that the interaction energy should drop to zero for film thicknesses below ~15 nm. In addition, an unusually large H-induced lattice expansion has been reported,[6] and the maximum out of plane lattice parameter change increases for thinner films.[3] No previous measurements have been done to address the role of the initial strain state of the Nb(110)-layers on the H-H-interaction. The possibility of controlling the strain states of the constituents, by varying their thickness ratio, makes Nb/W(110)-superlattices suitable for this purpose. Furthermore, the superlattices can be loaded and un-loaded with H to more than $\langle H/Nb\rangle=0.5$ without hysteresis effects, which seldom is the case for thin films. Therefore, in order to determine the thermodynamics of H in Nb(110) in the extreme thin limit (~2.8 nm), and to clarify the role of the strain state of the host-lattice on the H-H-interaction, we have studied the H uptake of four different Nb/W(110) samples. The thicknesses of the Nb-layers ($D_{Nb}=12$ ML) are equal for all samples, whereas the W-layers thicknesses ($D_W=3$, 8, 13 and 18 ML) are varied, and thereby generating an increasing bi-axial compressive strain in the Nb-layers. This particular sample series, thus, enables separation of finite-size-, and strain-state effects on the H-H-interaction.

II. EXPERIMENTAL DETAILS

A. Sample growth and characterization

Epitaxial Nb/W(110) superlattices were deposited by dc-magnetron sputtering. The depositions were carried out in 99.999999% pure Ar gas at a pressure of 2.25×10^{-3} mbar. The background pressure of the deposition chamber was in the 10^{-10}-mbar range. The targets were 99.95% pure Nb and W, and the substrates were $0.5\times10\times10$ mm^3, polished (110), *a*-cut, Al_2O_3 single crystals. Prior to the growth, the substrate was preheated for 10 min at 1173 K, and the target surfaces were sputter cleaned for 2 min. The growth temperature, 1073 K, was monitored using a IR pyrometer. Four samples were made, each consisting of 30 bilayer repetitions. The thicknesses of the Nb layers were kept constant and equal to 12 ML, while the W-layer thicknesses were varied among the samples from 3 to 18 ML.

X-ray diffraction (XRD) measurements were performed, using a Philips PW1820 powder diffractometer with an accuracy of 0.01° in 2θ. $\theta-2\theta$ XRD with Cu-$K\alpha$ radiation was carried out in the high-angle region ($30°-50°2\theta$) [see

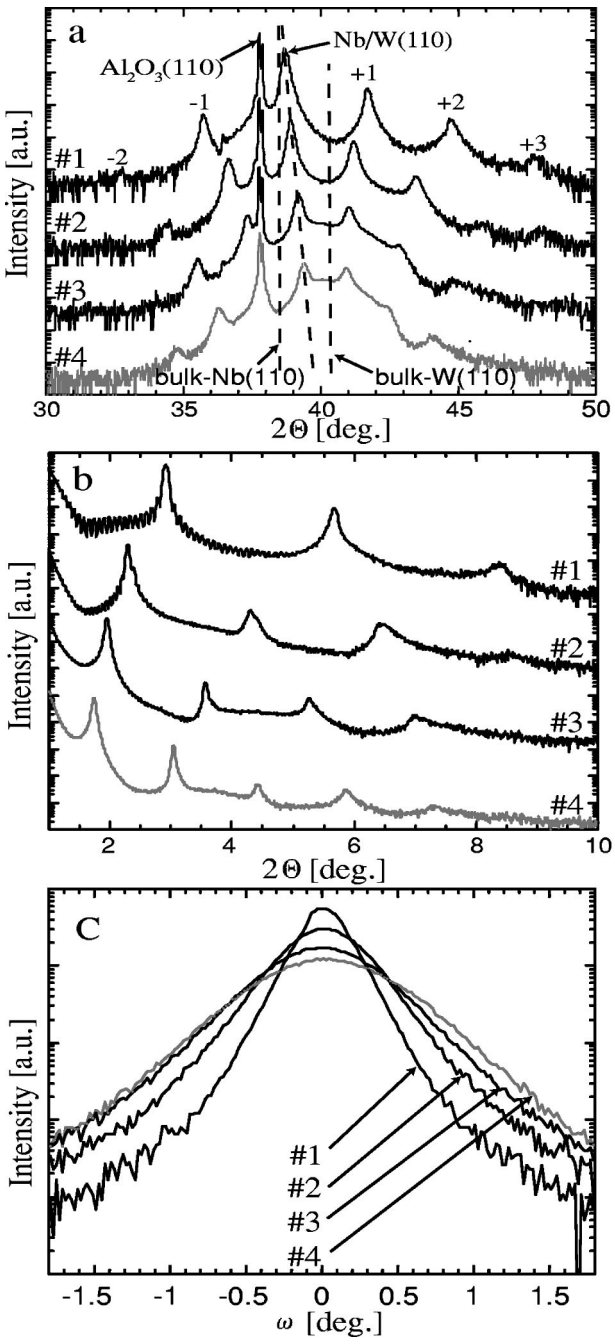

FIG. 1. X-ray diffraction patterns of Nb(D_{Nb} = 12 ML)/W(D_W)(110) superlattices. The four different scans corresponds to (#1) D_W=3, (#2) D_W=8, (#3) D_W=13, and (#4) D_W=18. (a) High angle diffraction patterns. 2–3 superlattice satellites (the order is marked as $\pm n$) are observed on both sides of the Nb/W(110) peak. The position of the bulk Nb(110), W(110), and Al_2O_3(110) Bragg angles are inserted for comparison. (b) Low angle diffraction patterns. Up to five superlattice peaks are visible, as well as finite-size oscillations at low angles. (c) Rocking scan (ω scan) around the main peak in the high angle pattern. For a discussion on the quality of the samples, see text.

Fig. 1(a)], and in the low-angle region ($1°-10°2\theta$) [see Fig. 1(b)]. Rocking curves were also measured on the Nb/W(110) peak; see Fig. 1(c). The high-angle patterns show, as expected, decreasing average Nb/W(110) lattice spacing for higher W contents: 2.327, 2.315, 2.298, and 2.287 Å, for the D_W=3, 8 ,13 and 18 ML sample respectively.

110 and 100 pole figures were recorded using a Philips MRD operated with (low resolution) parallel beam x-ray optics. The high angle spectra and the pole figures confirm that the films are truly epitaxial. However, in the high angle range a broader peak, centered between the Bragg angles for Nb and W bulk, is clearly visible for the sample with the thickest W layers [see Fig. 1(a)], and indicates that parts of the film have relaxed to the bulk lattice parameter of the constituents.

The rocking curves of the Nb/W(110) peak show an uncorrected broadening (full width at half maximum) of 0.26°, 0.50°, 0.72°, and 0.84° for the D_W=3, 8, 13, and 18 samples, respectively. The appearance of the broad peak for the D_W=18 sample, together with the broadening of the rocking curves, illustrate a deteriorating crystalline quality and the generation of higher defect concentrations, as the W-layer thickness is increased.

The low angle measurements show 3–5 superlattice peaks in the region from 1°–10° in 2θ. At very low angles ($0°-3°2\theta$), oscillations from the total film thickness can be seen for the two thinnest samples. The broadening of the superlattice peaks at higher angles, which is clearly seen for all samples, implies fairly large variations of the bilayer thicknesses. The average bi-layer thickness ($\Lambda = D_{Nb} + D_W$) was deduced by simulation using the Philips Win-GIXA software[7] with the results; Λ = 31.6, 41.6, 51.3, and 61.6 Å, for the D_W=3, 8, 13, and 18 samples, respectively. The simulations also give an estimation of the interface roughness of approximately 2 Å for the two samples with thinner W layers, and 4 Å for the other samples.

B. *p-c-T* measurements

Details of the experimental setup for the *p-c-T* measurements (*p* is the equilibrium H_2-gas pressure, *c* is the H concentration, and *T* is the temperature) can be found elsewhere.[9,8] Before each measurement, the sample and the sample stage were heated in ultrahigh vacuum at 573 K for several hours, and flushed with (1 mbar) ultrapure H_2 gas. The H_2 gas used in the experiments, initially of 99.99998% purity, was additionally purified in two steps: First through a West Associates ULTRAPURE gas purifier, and thereafter by absorption in a metal-hydride powder. The residual partial pressures of all gases except H_2, as determined by a quadrupole mass spectrometer, were in the 10^{-10}-mbar range during all experiments. $p-(\Delta R/R_0)$ isotherms ($\Delta R/R_0$ is the resistance change during H loading, normalized to the resistance without H at 573 K) were then measured by varying the temperature between 573 and 393 K, and the H_2-gas pressure between 0.01 mbar and 1 bar. The loading of the superlattices was carried out, at constant H_2-gas pressure, by decreasing the temperature in steps of 20 K (see Fig. 2). The resistance was registered with a 830 Stanford Research lock-in amplifier (resolution 0.1 mΩ) using a four-point technique. The gas pressure was read by three different pressure transducers with full scale: 1, 133, and 1000 mbar respectively (the accuracy is 0.1% of the full scale). The

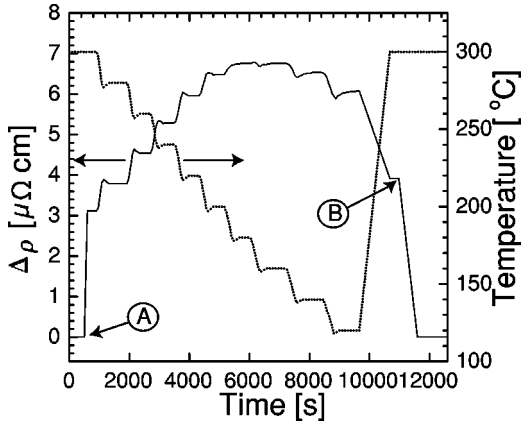

FIG. 2. The resistivity change when loading a Nb(12-ML)/W(13-ML)(110) superlattice at 10-mbar H_2-gas pressure. At the time marked *A*, the hydrogen gas is introduced, and at time *B* the sample cell is evacuated. The change of resistivity is reversible, i.e. the resistivity goes back to the initial value when evacuating the hydrogen.

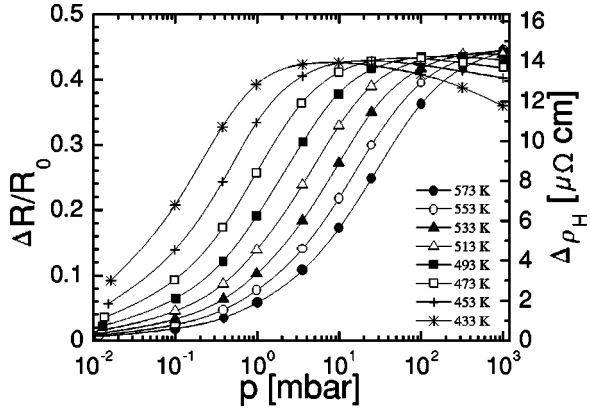

FIG. 3. $p-(\Delta R/R_0)$ isotherms of a Nb(12-ML)/W(3-ML)(110) superlattice. The resistivity change goes through a maximum, which also is seen for H in Mo/V superlattices.

sample temperature was measured by a chromel-alumel thermocouple and held within ± 1 K using a Eurotherm 94c temperature controller.

III. RESULTS AND ANALYSIS

A. Hydrogen induced resistivity change

A typical result for the resistivity change ($\Delta\rho_H$) of the superlattices during a H-absorption-desorption cycle is shown in Fig. 2. Notable is that the resistivity change is completely reversible, i.e., the resistivity returns to the initial value when all H is desorbed. $p-(\Delta R/R_0)$ isotherms for one of the superlattices are shown in Fig. 3. Similar to Mo/V superlattices,[8] ΔR exhibits a temperature dependent maximum. The maximum change of resistivity ($\Delta\rho_{H,max}$) can be fitted to the following expression:

$$\Delta\rho_{H,max}=A+BT[\mathrm{K}].$$

The coefficients *A* and *B* for the different samples are shown in Table I.

The resistivity change due to H in superlattices can be written as

$$\Delta\rho_H=\rho_i+\rho_{el},$$

where ρ_i is an impurity scattering term and ρ_{el} is the resistivity change due to H-induced modifications of the electronic structure. The electronic part has proved to make a significant contribution to the total resistivity change for some superlattices constituents combinations.[9] Instead of trying to separate the different terms, we express the concentration dependence of $\Delta R/R_0$ as a power series:

$$\frac{\Delta R}{R_0}=\sum_{i=1}^{\infty} a_i c^i. \tag{1}$$

Based on previous results[10] we truncate terms higher than second order in Eq. (1), i.e.,

$$\frac{\Delta R}{R_0}=a_1 c+a_2 c^2. \tag{2}$$

Proceeding as in Ref. 9 the following expression is obtained from Eq. (2):

$$c=c_{\Delta R_{max}}\pm c_{\Delta R_{max}}\left(1-\frac{\Delta R}{\Delta R_{max}}\right)^{1/2}, \tag{3}$$

where $c_{\Delta R_{max}}$ is the H to Nb atomic ratio at maximum resistance change. The actual H to M atomic ratio, at resistance maximum, was measured by $^1H(^{15}N,\alpha\gamma)^{12}$ nuclear reaction (see Table II), and $c_{\Delta R_{max}}$ is estimated to ~ 0.6 H per Nb atom. Equation (3) is then used to convert from the relative resistance change to the H to Nb atomic ratio ($\langle$H/Nb$\rangle$).

TABLE I. The temperature dependence of the maximum change of resistivity ($\Delta\rho_{H,max}$) during H loading of Nb/W(110)-superlattices. The change of $\Delta\rho_{H,max}$ with temperature appears to be linear and the coefficients *A* and *B* are the result from fitting the data to: $\Delta\rho_{H,max}=A+BT[\mathrm{K}]$.

L_{Nb}/L_W [ML]	*A* [$\mu\Omega$ cm]	*B* [$n\Omega$ cm K^{-1}]
12/3	11.6(5)	5.27(5)
12/8	9.6(2)	2.9(5)
12/13	5.2(1)	3.3(5)
12/18	1.0(5)	5.6(6)

TABLE II. Results from nuclear resonance analysis for samples loaded at the maximum resistivity change. The table includes the hydrogen to metal atomic ratio [H/M] and the average hydrogen to Nb atomic ratio $\langle$H/Nb$\rangle$.

L_W[ML]	[H/M]	$\langle$H/Nb$\rangle$	*T*[K]
8	0.36 ± 0.01	0.60	533
18	0.23 ± 0.01	0.58	493

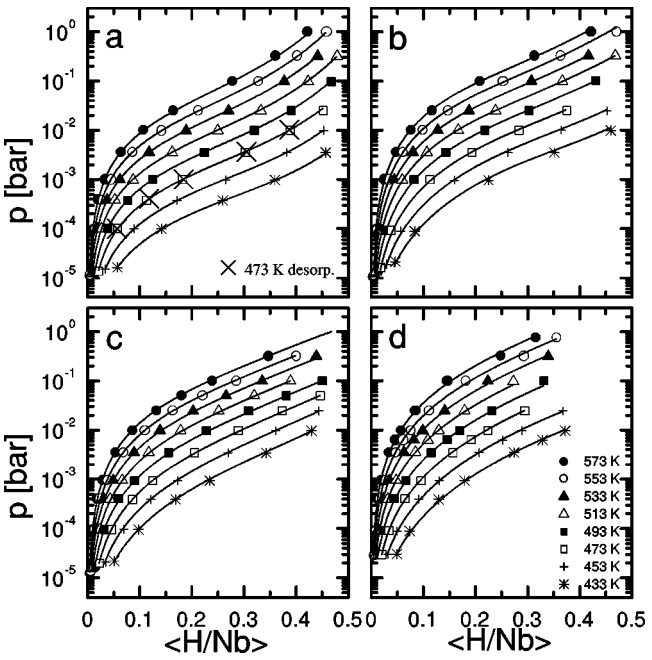

FIG. 4. The solution isotherms of hydrogen in Nb(D_{Nb} =12-ML)/W(D_W)(110) superlattices. (a) D_W=3 ML, (b) D_W =8 ML, (c) D_W=13 ML, and (d) D_W=18 ML. The solid lines are the best fits using Eq. (9).

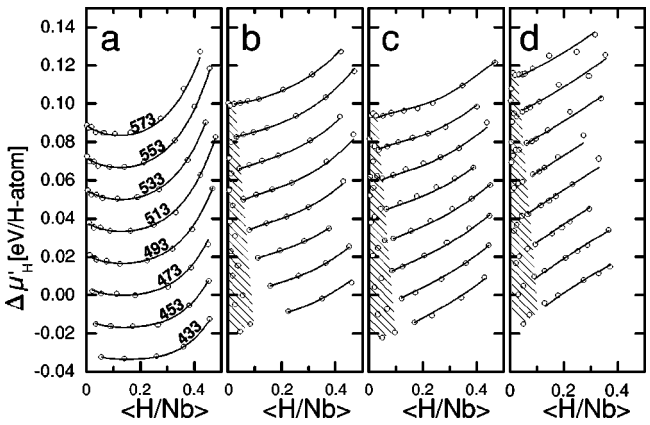

FIG. 5. The relative chemical potential minus the ideal partial configurational chemical potential for Nb(D_{Nb}=12 ML)/W(D_W) ×(110) superlattices at different temperatures. (a)–(d) corresponds to different thickness of the W layers: (a) D_W=3 ML. (b) D_W =8 ML. (c) D_W=13 ML (d) D_W=18 ML. The temperatures [in K] are as indicated in (a). The solid lines represent least-square fits to Eq. (9), using terms to fourth order in *c*. For the hatched areas, see the text.

B. Hydrogen solubility isotherms

The solution isotherms, as deduced from the $p-(\Delta R/R_0)$ isotherms [using Eq. (3)], are presented in Fig. 4. A comparison between the measured relative chemical potential ($\Delta\mu_H = k_B T \ln\sqrt{p}$, see below), at 573 K, for the superlattices and bulk Nb (Ref. 11) is provided in Fig. 6(a). The result reveals a lowered solubility (i.e., higher $\Delta\mu_H$), for the superlattices compared to bulk Nb. The trend in $\Delta\mu_H$, between the samples, is toward lower solubility as the W-layer thickness is increased, except that the D_W=13 sample has a slightly higher solubility than the D_W=8 sample.

For the least strained sample [see Fig. 4(a)] inflection points of the isotherms can be observed. Traditionally these have been used to mark the critical concentration for the $\alpha-\alpha'$ transition in Nb.[3] The point of inflection ($\langle H/Nb\rangle_{ifl.}$) is temperature dependent, varying from $\langle H/Nb\rangle_{ifl.}=0.24$ at 573 K to $\langle H/Nb\rangle_{ifl.}=0.30$ at 413 K. This temperature dependency, which is not seen for bulk Nb, is a consequence of the highly un-linear concentration dependency of the partial enthalpy of solution [see Fig. 6(b)].

The relative chemical potential minus the ideal partial configurational chemical potential ($\Delta\mu_H'$; see below) for the different samples is shown in Fig. 5. In this representation, the low concentration behavior of the solubility isotherms is more clearly visible. The increased defect density for the superlattices with thicker W layers (see Sec. II) is expected to be reflected in the solubility. In particular, vacancies should effect the H uptake at a low H concentration, as those are energetically favorable for H to occupy.[12] This is also observed for the D_W=8–18 samples at concentrations up to $\langle H/Nb\rangle \simeq 0.1$ (marked as hatched areas in Fig. 5). Similar effects in bulk metal-hydrogen alloys are reported in the literature; see Ref. 13 and references therein.

C. Thermodynamic model, $\Delta\overline{H}_H$ and $\Delta\overline{S}_H$

The relative partial enthalpy ($\Delta\overline{H}_H$) and entropy ($\Delta\overline{S}_H$) can be derived from *p-c-T* measurements through the expression[14]

$$\Delta\mu_H(c,T) = k_B T \ln\sqrt{p} = \Delta\overline{H}_H - T\Delta\overline{S}_H, \tag{4}$$

where

$$\Delta\overline{H}_H = \overline{H}_H - \frac{1}{2}\overline{H}^0_{H_2}, \tag{5}$$

$$\Delta\overline{S}_H = \overline{S}_H - \frac{1}{2}\overline{S}^0_{H_2}. \tag{6}$$

In Eqs. (5) and (6), $\overline{H}^0_{H_2}$ and $\overline{S}^0_{H_2}$ are the partial enthalpy and entropy of H_2 gas at the reference state (i.e., p =1013 mbar), respectively, and $\overline{H}_H$ and $\overline{S}_H$ are the respective partial enthalpy and entropy of the dissolved H. Proceeding as in Ref. 14, we subtract the ideal partial configurational entropy, $\overline{S}^{ic}_H = -k_B \ln[c/(6-c)]$, from Eq. (4), which upon rearrangement can be written as

$$\Delta\mu_H' = k_B T \ln[\sqrt{p}(6-c)/c] = \Delta\overline{H}_H - T\Delta\overline{S}_H', \tag{7}$$

where

$$\Delta\overline{S}_H' = \Delta\overline{S}_H - \overline{S}^{ic}_H. \tag{8}$$

$\Delta\overline{H}_H$ and $\Delta\overline{S}_H'$ can be modeled as polynomials in *c*, i.e.,

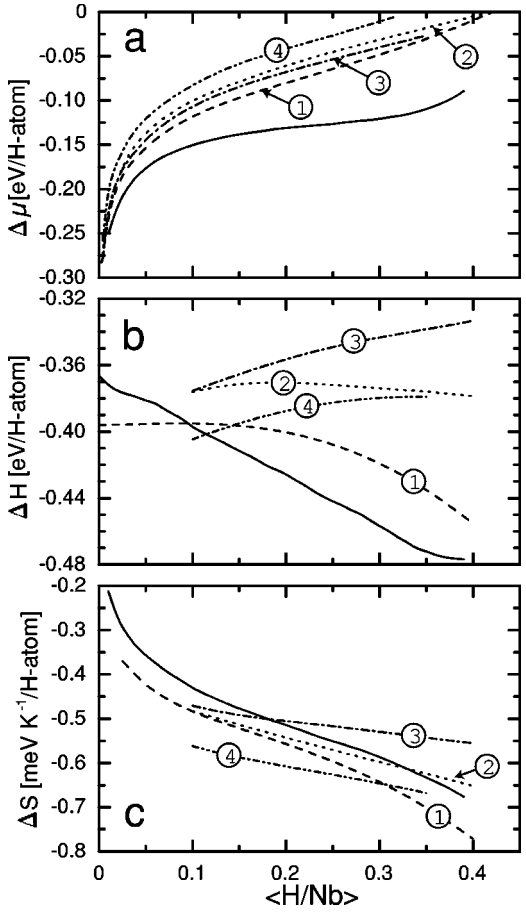

FIG. 6. The concentration dependence of $\Delta\mu_{\mathrm{H}}$ (measured at 573 K), $\Delta\overline{H}_{\mathrm{H}}$, and $\Delta\overline{S}_{\mathrm{H}}$ [as deduced from Eq. (9)], for Nb(D_{Nb} = 12 ML)/W(D_{W}=3–18 ML)(110) superlattices. The different lines correspond to (#1) $D_{\mathrm{W}}=3$, (#2) $D_{\mathrm{W}}=8$, (#3) $D_{\mathrm{W}}=13$, and (#4) $D_{\mathrm{W}}=18$. The solid lines are for bulk Nb (Ref. 11).

$$\Delta\mu'_{\mathrm{H}}(c,T)=\sum_{m,n=0}^{M,N}(h_n-T_m s_n)c_m^n, \tag{9}$$

where $M+1$ is the number of solubility data points, N is the order of the polynomials, and h_i and s_i are temperature independent coefficients.

The concentration dependence of $\Delta\overline{H}_{\mathrm{H}}$ and $\Delta\overline{S}_{\mathrm{H}}$, as deduced by fitting (i.e. minimizing the least-square error) the experimental data to Eq. (9) to fourth order in c, and a comparison with bulk Nb,[11] is plotted in Figs. 6(b) and 6(c), respectively. Within the hatched areas in Fig. 5, the above model [Eq. (9)] could not be applied due to temperature dependencies in $\Delta\overline{H}_{\mathrm{H}}$ and/or $\Delta\overline{S}_{\mathrm{H}}$.

For the $D_{\mathrm{W}}=3$ sample, the relative partial enthalpy at infinite dilution, $\Delta\overline{H}_{\mathrm{H}}{}^{0}\equiv h_0$ [in Eq. (9)] $=-0.396\pm0.010$ eV/H atom, is lowered (i.e., a more exothermic reaction) with $\sim$35 meV relative to bulk Nb. This result is in contrast to Nb/Mo(001) superlattices[15] and thin epitaxial Nb(110) films,[16] where the solution of H is reported to be more endothermic than in bulk Nb. The extrapolated values of $\Delta\overline{H}_{\mathrm{H}}{}^{0}$ for the $D_{\mathrm{W}}=8-13$ samples are, within the experimental accuracy, equal to the $D_{\mathrm{W}}=3$ sample, while for the $D_{\mathrm{W}}=18$ sample $\Delta\overline{H}_{\mathrm{H}}{}^{0}$ is evidently more negative.

At intermediate and high concentrations, variations of $\Delta\overline{H}_{\mathrm{H}}$ and $\Delta\overline{S}_{\mathrm{H}}$ with c are due to the interaction between the dissolved H. The slope of $\Delta\overline{H}_{\mathrm{H}}$ versus c can be interpreted as the H-H interaction energy ($u_{\mathrm{H\text{-}H}}$), while the slope of $\Delta\overline{S}_{\mathrm{H}}$ versus c contains information regarding H-H correlations.

In the low concentrations range, $0<\langle\mathrm{H/Nb}\rangle<0.12$, $u_{\mathrm{H\text{-}H}}$ is close to zero for the $D_{\mathrm{W}}=3$ sample. As the concentration is increased, $u_{\mathrm{H\text{-}H}}$ is gradually becoming more attractive, and reaches -0.36 ± 0.05 eV/H atom at $\langle\mathrm{H/Nb}\rangle=0.4$, which is comparable to bulk Nb (-0.3 eV/H atom).[11] For the $D_{\mathrm{W}}=8$ sample, $u_{\mathrm{H\text{-}H}}$ is repulsive at low concentrations, but changes to slightly attractive above $\langle\mathrm{H/Nb}\rangle\simeq0.2$, while for the $D_{\mathrm{W}}=$13-18 samples, $u_{\mathrm{H\text{-}H}}$ is repulsive over the whole measured concentration range ($0.1<\langle\mathrm{H/Nb}\rangle<0.4$).

At low concentrations, the entropy data for all samples reveal a more ordered solution than bulk Nb. When the concentration is increased the slope of $\Delta\overline{S}_{\mathrm{H}}$ versus c for the $D_{\mathrm{W}}=3$ sample follows the bulk-Nb behavior, while for the $D_{\mathrm{W}}=8-18$ samples, the slope is monotonically decreasing with concentration.

The shift towards more negative values of both $\Delta\overline{H}_{\mathrm{H}}$ and $\Delta\overline{S}_{\mathrm{H}}$ for the $D_{\mathrm{W}}=18$ sample, in comparison with the other samples, indicates a more attractive M-H interaction and reduced degrees of freedom of the dissolved H. The reason for this is, at this moment, unclear. One possible explanation involves H-absorption in the relaxed parts of the Nb layers, which according to the x-ray spectra (see above), are largest for this sample, but a further exploration of these effects has to be postponed.

The critical temperature (T_{c}) and concentration (c_{c}), for the $\alpha-\alpha'$ transition can be determined using the following definition of a critical point:

$$\left.\frac{\partial\mu}{\partial c}\right|_{p_{\mathrm{c}},T_{\mathrm{c}}}=\left.\frac{\partial^2\mu}{\partial c^2}\right|_{p_{\mathrm{c}},T_{\mathrm{c}}}=0. \tag{10}$$

Using the polynomials for $\Delta\overline{H}_{\mathrm{H}}$ and $\Delta\overline{S}_{\mathrm{H}}{}'$, obtained from the solubility data, in Eq. (10) gives $T_{\mathrm{c}}=287$ K and $c_{\mathrm{c}}=0.39$ H per Nb atom for the $D_{\mathrm{W}}=3$ sample. For the $D_{\mathrm{W}}=8-18$ samples, no transition of this kind could be verified.

IV. DISCUSSION

The main motivation for studying H-H interactions in thin films and superlattices is the possibility to address the effect from the finite thickness of the host material on the critical behavior and the phase diagram of the H lattice gas. Apart from the finite-size effects, the coupling between the film and substrate, the presence of the H free layers, as well as the strain state of the host-lattice, are also expected to alter the phase diagram. The absence of hysteresis effects in the resistivity change ($\Delta\rho_{\mathrm{H}}$), despite loading the samples to more than $\langle\mathrm{H/Nb}\rangle=0.5$, which also is the case for Mo/VH$_x$- and Fe/VH$_x$-superlattices ($x=0-1$), is a strong indication that no in-plane expansion is taking place when loading the

samples, i.e., the Nb-layers are totally ''clamped'' in the film plane (uniaxial expansion). The role of different elastic boundary conditions on the H-H-interaction was first recognized by Alefeld.[17] A general discussion on the consequences of uniaxial expansion on the H-H-interaction is found in Ref. 18.

The higher defect concentration in the samples with thicker W layers is mainly affecting the H-uptake in the low concentration range ($\langle H/Nb\rangle < 0.1$). It is, however, possible that a higher lattice defect concentration can affect the H-H interaction through its effect on the elastic constants. However, on an absolute scale, all the samples can be considered to have a good crystal quality. The essential difference between the $D_W = 3$–13 samples is the degree of compression of the Nb layers, while for the sample with thickest W layers ($D_W = 18$ ML) both the x-ray data and solubility data (see above) indicate a more complex structure. This is most likely related to a transition from a smooth layer by layer growth to a mixed three-dimensional (3D) and 2D growth mode, which results in increased variation of the layer thicknesses. A similar transition can be observed when increasing the V-layer thickness during sputtering of epitaxial Mo/V and Fe/V superlattices.[19,20]

A. Infinite dilution limit

The effect by the biaxial compression of the Nb layers on the solution energy can be theoretically assessed using the effective medium theory.[21,22] The energy difference between a H atom situated at a interstitial site in metal and a free H atom is written as

$$\Delta E = \Delta E_{\mathrm{eff}}^{\mathrm{hom}}(\overline{n_0}) + \Delta E^{\mathrm{hyb}}, \tag{11}$$

where $\Delta E_{\mathrm{eff}}^{\mathrm{hom}}(\overline{n_0})$ is the energy of a H atom in a homogeneous electron gas with density; $\overline{n_0} =$ the interstitial electron density (IED), and ΔE^{hyb} is the hybridization energy. The IED is expected to increase in the Nb/W(110) superlattices due to the compression of the Nb layers (the atomic volume of Nb can, using linear elasticity, be estimated to decrease with 1.3% for the $D_W = 3$-sample). Differentiating the parametrized version of $\Delta E_{\mathrm{eff}}^{\mathrm{hom}}(\overline{n_0})$ (Ref. 23) with respect to $\overline{n_0}$ gives[24]

$$\delta \Delta E_{\mathrm{eff}}^{\mathrm{hom}} = (796\overline{n_0} + 20.9)\,\delta\overline{n_0}. \tag{12}$$

If Eq. (12) is applied on the $D_W = 3$ sample, by assuming an equal number of valence electrons as bulk Nb, $\Delta\overline{H}_H{}^0$ should increase (more endothermic) with 22-meV/H atom relative the bulk Nb, which is in stark contrast to the experimentally determined differences in $\Delta\overline{H}_H{}^0$ (see Sec. III C). One plausible reason for the apparent contradiction is the different electronic boundary conditions of Nb layers in a Nb/W superlattice structure and bulk Nb, which certainly will affect the IED. The effect from the electronic boundary conditions on the IED of the V layers in Mo/V superlattices has proved to be significant.[25] Furthermore, the biaxial compressive strain makes the tetrahedral sites ($T_{x,y,z}$), which is the occupancy of H in bulk Nb (see Fig. 7), unequivalent. The *T* sites

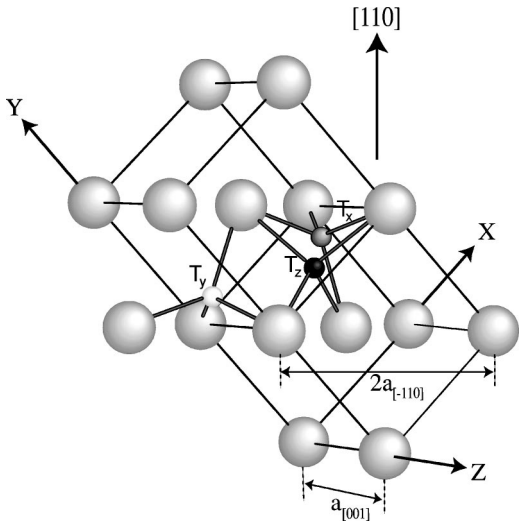

FIG. 7. The orientation and location of the tetrahedral (*T*) interstitial sites in a bcc lattice. The Nb/W superlattices used in this study are grown in the [110] direction. The strong adhesion of the Nb layers on the substrate and the (hydrogen-free) W layers excludes any hydrogen induced lattice expansion in the film plane. The in-plane lattice parameters $a_{\bar{1}10}$ and a_{001} are also shown.

in biaxially compressed Nb(110) layers can be divided into two groups, with different surroundings, i.e., $T_{x,y}$ and T_z.[26] A different site occupancy than bulk Nb should be reflected in the configurational entropy of the dissolved H; therefore a closer examination of $\Delta\overline{S}_H$ is justified.

The partial entropy of the dissolved H can be divided into configurational (*c*) and non-configurational (nc) entropy:

$$\overline{S}_H = \overline{S}_H^c + \overline{S}_H^{\mathrm{nc}}. \tag{13}$$

The configurational term is, at low H concentrations, equal to $-k_B\ln(c/\beta)$, where β is the number of interstitial sites per Nb atom and *c* is the *H*-concentration. The combination of Eqs. (13), (8), and (6) then gives the following relation as $c \to 0$:

$$\Delta\overline{S}'^0_H = k_B\ln(\beta/6) + \overline{S}_H^{\mathrm{nc0}} - \frac{1}{2}\overline{S}_{H_2}, \tag{14}$$

where $\Delta\overline{S}'^0_H$ and $\overline{S}_H^{\mathrm{nc0}}$ are the respective values for $\Delta\overline{S}'_H$ and $\overline{S}_H^{\mathrm{nc}}$ as $c \to 0$. The difference between $\Delta\overline{S}'^0_H \equiv s_0$ [in Eq. (9)] for the $D_W = 3$ sample and bulk-Nb (Ref. 11) is $\sim -0.08\ \mathrm{meV\,K^{-1}}$ per H atom. If one assumes small changes of $\overline{S}_H^{\mathrm{nc0}}$ compared to bulk, it is possible to infer a lower value of β in the Nb(110) layers compared to bulk Nb ($\beta = 6$), as an explanation for the shift in $\Delta\overline{S}'^0_H$. This could be a consequence of exclusive occupation of $T_{x,y}$ sites [$k_B\ln(4/6) = -0.035\ \mathrm{meV\,K^{-1}/H\ atom}$] or T_z sites [$k_B\ln(2/6) = -0.095\ \mathrm{meV\,K^{-1}/H\ atom}$], or a noneven distribution over the $T_{x,y,z}$ sites.

B. Strain dependency of the H-H interaction

In order to explore the relation between initial strain of the Nb(110) layers and $u_{H\text{-}H}$ in more detail, the in-plane lat-

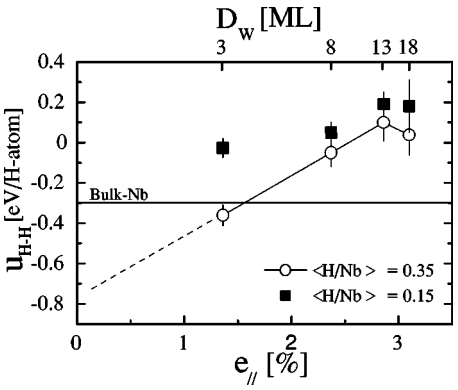

FIG. 8. Correlation between the initial in-plane strain, $e_{//}$, of the Nb(110) layers in Nb/W(110) superlattices and H-H interaction energy ($u_{\text{H-H}}$). $u_{\text{H-H}}$ is taken as the slope of $\Delta\overline{H}_{\text{H}}$ vs c, at two different concentrations. At $\langle \text{H/Nb} \rangle = 0.35$, $u_{\text{H-H}}$ is close to the bulk Nb value (Ref. 11) for the least strained sample ($D_{\text{W}}=3$ sample), and turns to repulsive in the $D_{\text{W}}=13$ sample. The influence of the initial strain on the H-H interaction is smaller at low concentrations. An extrapolation of $u_{\text{H-H}}$, at $\langle \text{H/Nb} \rangle = 0.35$, to zero strain (dashed line) gives $u_{\text{H-H}} \simeq -0.75$ eV/H atom.

tice parameters (i.e., $a_{\bar{1}10}$ and a_{001}; see Fig. 7) of the Nb layers in the different superlattices have to be estimated. Using the following expression for the elastic energy density of a deformed body:

$$w = \frac{1}{2} \sum_{ijkl} C_{ijkl} e_{ij} e_{kl}, \tag{15}$$

the energy per unit area (E/A) of a individual layer can, for small and homogeneous compression/expansion in the plane ($e_{xx}=e_{yy}=e_{\bar{1}10}/\sqrt{2}$ and $e_{zz}=e_{001}$), be obtained as

$$E/A = N\left[\frac{1}{2}(C_{11}+C_{12})e_{\bar{1}10}^2 + \sqrt{2}C_{12}e_{\bar{1}10}e_{001}\right], \tag{16}$$

where N is the layer thickness. The in-plane lattice parameters are then calculated using Eq. (16), and the elastic data from Ref. 27, by minimizing the total elastic energy of the film.

The relation between initial strain of the Nb layers and $u_{\text{H-H}}$ is shown in Fig. 8, where the interaction energy ($u_{\text{H-H}} = \partial\Delta\overline{H}_{\text{H}}/\partial c$) at two different concentrations is plotted against the in-plane strain $e_{//}=(a_{\bar{1}10}^{\text{b}}-a_{\bar{1}10}^{\text{sl}})/a_{\bar{1}10}^{\text{b}}$, where $a_{\bar{1}10}^{\text{b}}$ and $a_{\bar{1}10}^{\text{sl}}$ correspond to the bulk (b) and calculated values for a perfectly strained superlattice (sl), respectively. At the lower concentration ($\langle \text{H/Nb} \rangle = 0.15$), $u_{\text{H-H}}$ is zero or repulsive regardless of the in-plane strain. This observation is in accordance with the prediction that the interaction energy should changes to repulsive for film thicknesses below ~ 15 nm,[3] since the thicknesses of the current Nb(110) structures are only ~ 2.8 nm. However, at the higher concentration ($\langle \text{H/Nb} \rangle = 0.35$), and lower compressive strain, $u_{\text{H-H}}$ is attractive and even exceeds bulk Nb. Furthermore, the estimated value of $u_{\text{H-H}}$ (by extrapolation) at zero strain reaches ~ -0.75 eV/H atom. Such a strong attractive H-H-interaction should, due to the intimate relation between elastic interaction and the H induced volume increase, be accompanied by an unusually large lattice expansion. This has, in fact, been reported by several research groups for H in epitaxial Nb(110) films.[3,6]

V. SUMMARY AND CONCLUSIONS

H solubility isotherms and the relative partial enthalpy ($\Delta\overline{H}_{\text{H}}$) and entropy ($\Delta\overline{S}_{\text{H}}$) of H in Nb/W(110) superlattices are presented. The H concentration was monitored by measuring the resistance change during H loading, which was linked to the average H concentration using the $^1\text{H}(^{15}\text{N},\alpha\gamma)^{12}\text{C}$ nuclear reaction. Of special interest was to determine the effect of different strain states of the host lattice on $u_{\text{H-H}}$. The strain dependency of the H solubility was separated from the finite-size effects, using a sample series consisting of four samples with a constant thickness of the H-dissolving layers ($D_{\text{Nb}}=12$ ML), but with a varying W-layer thickness ($D_{\text{W}}=3$–18 ML). For the $D_{\text{W}}=3$ sample, $\Delta\overline{H}_{\text{H}}$ and $\Delta\overline{S}_{\text{H}}' = \Delta\overline{S}_{\text{H}} - \overline{S}_{\text{H}}^{\text{ic}}$, at infinite dilution, indicate a different interstitial site occupancy of H than bulk Nb. The biaxial compression was found to have a large influence on the concentration dependence of $\Delta\overline{H}_{\text{H}}$ and $\Delta\overline{S}_{\text{H}}$, i.e., on the H-H interaction. At $\langle \text{H/Nb} \rangle = 0.35$, $u_{\text{H-H}}$ changes from attractive (-0.36 eV/H atom) to repulsive (0.10 eV/H atom), as the W-layer thickness is increased from 3 to 13 ML. The extrapolated value for $u_{\text{H-H}}$, at zero initial strain, reaches ~ -0.75 eV/H atom. This could be related to the large lattice expansion reported for Nb(110) structures upon H loading.

ACKNOWLEDGMENTS

The work was financially supported by NFR, which is gratefully acknowledged.

*Electronic address: stefan.olsson@fysik.uu.se

[1] H. Wagner and H. Horner, Adv. Phys. **23**, 587 (1974).
[2] H. Zabel and H. Peisl, Phys. Rev. Lett. **42**, 511 (1979).
[3] G. Song, M. Geitz, A. Abromeit, and H. Zabel, Phys. Rev. B **54**, 14 093 (1996).
[4] R. Feenstra, G. de Bruin-Hordijk, H. Bakker, R. Griessen, and D. de Groot, J. Phys. F: Met. Phys. **13**, L13 (1983).
[5] B. Hjörvarsson, G. Andersson, and E. Karlsson, J. Alloys Compd. **253**, 51 (1997).
[6] P.M. Reimer, H. Zabel, C. Flynn, K. Ritley, J. Steiger, S. Blässer, and A. Weidinger, Z. Phys Chem. **181**, 367 (1993).
[7] D.K.G. de Boer, Phys. Rev. B **44**, 498 (1991).
[8] F. Stillesjö, S. Olafsson, P. Isberg, and B. Hjörvarsson, J. Phys.: Condens. Matter **7**, 8139 (1995).
[9] S. Olsson, P. Blomquist, and B. Hjörvarsson, J. Phys.: Condens. Matter **13**, 1685 (2001).
[10] G. Andersson, B. Hjörvarsson, and H. Zabel, Phys. Rev. B **55**, 15 905 (1997).

[11] E. Valeckis and R. Edwards, J. Phys. Chem. **9**, 73 (1969).
[12] J.K. Nörskov and F. Besenbacher, J. Less-Common Met. **130**, 475 (1987).
[13] W.A. Oates and T.B. Flanagan, Prog. Solid State Chem. **13**, 193 (1981).
[14] T. Flanagan and W. Oates, Ber. Bunsenges **76**, 706 (1972).
[15] G. Reynaldsson, H. P. Gislason, S. Olafsson, and B. Hjörvarsson (unpublished).
[16] G. Song, Ph.D. thesis, Ruhr-Universität Bochum, Bochum, 2000.
[17] G. Alefeld, Ber. Bunsenges. Phys. Chem. **76**, 746 (1972).
[18] H. Zabel and B. Hjörvarsson, in *Progress in Hydrogen Treatment of Materials*, edited by V.A. Goltsov (Donetsk State Technical University, Donetsk, 2001).
[19] J. Birch, Y. Yamamoto, L. Hultman, G. Radnoczi, and J.-E. Sundgren, Vacuum **41**, 1231 (1990).
[20] P. Isberg, B. Hjörvarsson, R. Wäppling, E. Svedberg, and L. Hultman, Vacuum **48**, 483 (1997).
[21] J. Nörskov and N.D. Lang, Phys. Rev. B **21**, 2131 (1980).
[22] J. Stott and E. Zaremba, Phys. Rev. B **22**, 1564 (1980).
[23] J. Nörskov, Phys. Rev. B **26**, 2875 (1982).
[24] B. Hjörvarsson, S. Ólafsson, F. Stillesjö, and E. Karlsson, Z. Phys. Chem. **181**, 343 (1993).
[25] S. Papadia, K. Karlsson, P. Nilsson, and T. Jarlborg, Phys. Rev. B **45**, 1857 (1992).
[26] J. Öhrmalm, G. Andersson, J. Birch, and B. Hjörvarsson, J. Alloys Compd. **285**, 21 (1999).
[27] G. Simmons and H. Wang, *Single Crystal Elastic Constants and Calculated Aggregate Properties: A Handbook* (MIT Press, Cambridge, MA, 1971).